Heliyon 10 (2024) e29960

Contents lists available at ScienceDirect

Heliyon

journal homepage: www.cell.com/heliyon

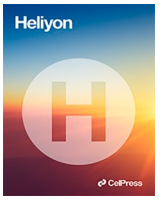

Research article

A novel seasonal grey prediction model with fractional order accumulation for energy forecasting

Huiping Wang *, Yiyang Li

Resource Environment and Regional Economic Development Research Center, Xi'an University of Finance and Economics, Xi'an, 710100, China

ARTICLE INFO

Keywords:
Seasonal prediction model
FSGM (1,1,α)
Energy forecasting
Fractional order accumulation

ABSTRACT

To accurately predict sequence data with seasonal characteristics, we combine data restart technology and fractional order accumulation into a novel seasonal grey model (FSGM (1,1, α)). The particle swarm optimization (PSO) algorithm is used to solve the fractional order and background value coefficients of the model, and the effectiveness of FSGM (1,1, α) is verified using three cases. Finally, we use FSGM (1,1, α) to predict quarterly electricity generation in Beijing and Henan Province and quarterly petroleum coke production in China from 2023 to 2027. The research results indicate that, first, FSGM (1,1, α) is reasonable and effective and has the ability to accurately capture the dynamic trend of seasonal data. Second, compared with the grey model (GM (1,1)), seasonal grey model (SGM (1,1)), data grouping grey model (DGGM (1,1)), data grouping seasonal model (DGSM (1,1)), and data grouping seasonal time model (DGSTM (1,1)), which have seasonal characteristics, FSGM (1,1, α) can better fit the original data, achieve higher prediction accuracy, and perform better. Third, from 2023 to 2027, it is predicted that there will be no significant change in Beijing's electricity generation, and the current stable trend will be maintained. Both the power generation in Henan Province and the petroleum coke production in China will steadily increase to a certain extent, with obvious seasonal cyclical fluctuations. Notably, the power generation and petroleum coke production in Henan Province in the fourth quarter of 2027 will increase by 11.50 % and 10.93 %, respectively, compared to those in the fourth quarter of 2023.

1. Introduction

Accurate prediction of economic operation data can provide valuable information for formulating medium- and long-term policies [1]. However, in practice, various complex factors, especially seasonal and uncertain factors, often lead to biased prediction results [2]. Seasonal fluctuations in economic data are common, mainly due to factors such as changes in the supply and demand, variations in economic activities and climate change, which directly or indirectly lead to systematic, cyclical or irregular changes in statistical indicators. Generally, seasonal fluctuation time series data exhibit both long-term trends and seasonal volatility, as well as local random oscillations [3]. In macroeconomics, seasonal data mainly include quarterly and monthly data, which are often highly variable, while annual data display comparatively higher stability. Therefore, seasonal data can capture the underlying information associated with rapid environmental changes, and modeling can effectively avoid the loss of some key information. Seasonal data typically exhibit similar trends, volatility and randomness in different cycles, undoubtedly increasing the difficulty of prediction [4].

* Corresponding author.
E-mail address: wanghuiping@xaufe.edu.cn (H. Wang).

https://doi.org/10.1016/j.heliyon.2024.e29960
Received 21 January 2024; Received in revised form 14 April 2024; Accepted 18 April 2024
Available online 20 April 2024

Common seasonal data include fine particulate matter ($PM_{2.5}$) pollution data [5], renewable energy consumption data [6], electricity demand data [7], natural gas consumption and production data [8,9], and residential electricity consumption data [10].

The complex data characteristics of seasonal time series pose significant challenges to the construction of corresponding prediction models. Therefore, scholars have continuously explored and proposed various prediction methods. At present, seasonal data prediction methods can be divided into three main categories. Statistical analysis methods fall into the first category and include exponential smoothing models [11], autoregressive integrated moving average (ARIMA) models [12], seasonal ARIMA (SARIMA) models [13], and SARIMA–support vector regression (SVR) models [14]. These methods use mathematical models for prediction based on the trend of historical data changes and relationships with influencing factors. The second category includes artificial intelligence models, such as artificial neural networks (ANNs) [15,16], support vector machines (SVMs) [17], random forests, and extreme gradient boosting [18]. These methods are used to obtain the inherent mathematical characteristics of historical data based on complex algorithms or programs and corrections to the prediction model in real time, thus avoiding the limitations of single models for predicting complex seasonal series. The third category includes the grey model series. Due to the complexity and uncertainty of influencing factors, seasonal fluctuation data are often characterized by unclear structures and uncertain behavior. The grey model is a commonly used mathematical modeling method for studying the prediction of uncertain systems. The existing seasonal grey prediction models include the seasonal grey model (SGM (1,1)) [19], discrete grey seasonal model (DGSM (1,1)) [2], data grouping seasonal time model (DGSTM (1,1)) [20], average weakening buffer operators–data grouping grey model (AWBO-DGGM (1,1)) [21], particle swarm optimized fractional-order-accumulation discrete grey seasonal model (PFSM(1,1)) [22], data restacking–seasonal factor grey model (DR-SFGM) [6], seasonal division-based grey seasonal variation index (OSGSVI) [23], and weighted average weakening buffer operator–fractional order accumulation seasonal grouping grey model (WAWBO-FSGGM (1,1)) [24], which are widely used in many fields. In addition, due to their broad applicability, small sample size requirement, and high accuracy, grey prediction models are widely used after continuous optimization and improvement. For example, water consumption [25], hydroelectricity consumption [26], renewable energy production [27], air pollution (Wang, Xie, & Yang, 2022) [5], air quality [28], power generation [29], urban per capita consumption [30], electricity demand [7], renewable energy generation [31], carbon emissions [32], residential electricity consumption [10], passenger flow volume [33], high-tech industry values [34], new energy vehicle sales [35], and natural gas production and consumption [36] have been predicted.

In a grey model modeling problem, to achieve optimization, many scholars have improved previous models and applied these new versions to predict seasonal data, which has expanded the application scope of grey models [5–10]. Moreover, scholars have developed different methods for the processing of seasonal data [20,21,24]. A seasonally fluctuating time series is different from a random-oscillation series, such as stock series, and has three major characteristics: trend, periodicity, and volatility. Therefore, effective mining of the characteristics of seasonally fluctuating data is the basis for constructing a reasonable prediction model. Although many studies have used grey models to predict seasonal data, these studies still have certain shortcomings in terms of the model structure and parameter-solving ability, making it difficult to accurately identify seasonal features. In response to this deficiency, a new modeling concept is proposed in this study. By combining the fractional order accumulation method with data restart technology, a new grey seasonal model, namely, FSGM (1,1, α), is developed to predict quarterly electricity generation in Beijing and Henan and petroleum coke production in China from 2023 to 2027. The contributions of this study are as follows:

(1) In this paper, a novel seasonal grey prediction model FSGM (1,1, α) is developed by combining existing data processing methods, namely, the data restart technique and fractional order accumulation method, and is applied for seasonal data prediction.
(2) In the modeling process of the FSGM (1,1, α), by solving for the development coefficient a of FSGM (1,1, α), four groups are distinguished by seasonal factors and combined to obtain a new form of matrix B, resulting in a more reliable set of parameter values.
(3) The verification results through three cases show that FSGM (1,1) with seasonal characteristics has higher prediction accuracy than GM (1,1), SGM (1,1), DGGM (1.1), DGSM (1,1), and DGSTM (1,1) models, and can better describe the trend of data changes.
(4) FSGM (1,1, α) is applied to predict quarterly electricity generation in Beijing and Henan Provinces and quarterly petroleum coke production in China from 2023 to 2027.

The organizational structure of this article is as follows. Section 2 introduces the construction and solution processes of FSGM (1,1, α), data restart techniques, optimization methods for background value coefficients, and error evaluation standards for the model. Section 3 verifies the feasibility and effectiveness of FSGM (1,1, α) through three case studies. In Section 4, electricity generation in Beijing and Henan Provinces and petroleum coke production in China from 2023 to 2027 are predicted. Section 5 provides the conclusion of this article.

2. Construction of FSGM (1,1, α)

This section first introduces the traditional GM (1,1) model, then describes the modeling and solving process of the newly proposed FSGM(1,1, α) model, as well as the PSO algorithm. Then, a flowchart of the FSGM (1,1) model is drawn, and error evaluation criteria are provided.

2.1. Traditional GM (1, 1)

For the sequence $X^{(0)} = (x^{(0)}(1), x^{(0)}(2), \cdots, x^{(0)}(n))$, where $x^{(0)}(k) \geq 0, k = 1, 2, \cdots, n$, $X^{(1)} = (x^{(1)}(1), x^{(1)}(2), \cdots, x^{(1)}(n))$ is a first-order accumulation generation operator (1-AGO) for $X^{(0)}$, where

$$x^{(1)}(k) = \sum_{i=1}^{k} x^{(0)}(i), k = 1, 2, 3, \cdots, n \tag{1}$$

$Z^{(1)}$ is used to generate a sequence of immediately adjacent means for $X^{(1)}$, where

$$z^{(1)}(k) = 0.5x^{(1)}(k) + 0.5x^{(1)}(k-1), k = 1, 2, 3, \cdots, n \tag{2}$$

By assuming that the sequence $(X^{(0)}, X^{(1)}, Z^{(1)})$ is as shown in the above definition, the basic form of GM(1,1) is

$$x^{(0)}(k) + az^{(1)}(k) = b, k = 1, 2, \cdots n \tag{3}$$

In this model, b is referred to as the grey action term, and a is the development coefficient. The column of least square values estimated for the model satisfies $[\widehat{a}, \widehat{b}] = (B^T B)^{-1} B^T Y$, where

$$B = \begin{bmatrix} -z^{(1)}(2) & 1 \\ -z^{(1)}(3) & 1 \\ \vdots & \vdots \\ -z^{(1)}(n) & 1 \end{bmatrix}, Y = \begin{bmatrix} x^{(1)}(2) \\ x^{(1)}(3) \\ \vdots \\ x^{(1)}(n) \end{bmatrix} \tag{4}$$

The whitening equation of GM(1,1) is

$$\frac{dx^{(1)}}{dt} + ax^{(1)} = b \tag{5}$$

Then, the solution to the whitening equation is

$$\widehat{x}^{(1)}(k) = \left(x^{(0)}(1) - \frac{b}{a}\right) e^{-a(k-1)} + \frac{b}{a}, k = 2, 3, \cdots, n. \tag{6}$$

The final reduced equation is

$$\widehat{x}^{(0)}(k) = \widehat{x}^{(1)}(k) - \widehat{x}^{(1)}(k-1) = (1 - e^{a})\left(x^{(0)}(1) - \frac{b}{a}\right) e^{-a(k-1)}, k = 2, 3, \cdots, n. \tag{7}$$

2.2. FSGM (1,1, α) model

2.2.1. Raw data processing based on restart technology

Currently, raw data are preprocessed using two main methods. First, seasonal factors are used to preprocess the data; for example, SGM (1,1) uses this technique. The seasonal factor $f_s(i)$ is a dimensionless parameter that reflects the average deviation of actual values

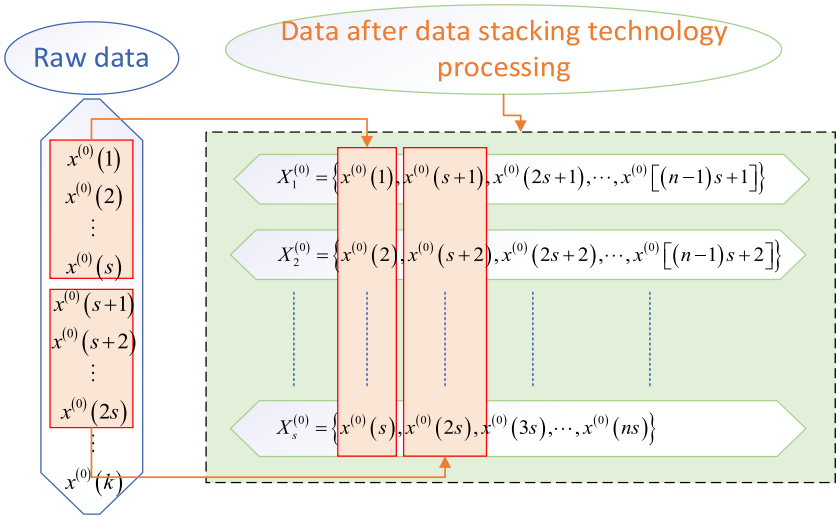

Fig. 1. The data restart process.

from trend values due to seasonal effects, and its formula is $f_s(i) = \bar{x}_M^{(0)}(i)/\bar{x}_{MN}^{(0)}(i)$, where M is the number of cycles in a year. If seasonal data are used, then $M = 4$; if monthly data are used, then $M = 12$. N represents the year of the i-th time point. $\bar{x}_M^{(0)}(i)$ and $\bar{x}_{MN}^{(0)}(i)$ represent the mean value of the quarter (or month) at the i-th time point and the total mean value of all quarters (or months), respectively.

Another approach is to use restart techniques to preprocess the raw data, mainly by clustering observation data from the same month or quarter into the same group to eliminate disturbances caused by seasonal factors [43]. After restart processing, the original observation results are retained for each set of data, but there are no seasonal characteristics within each group. Thus, the accuracy of subsequent predictions can be significantly improved. The data restart process is shown in Fig. 1.

In this article, a data restart method is used to process the raw sequence $X^{(0)} = (x^{(0)}(1), x^{(0)}(2), \cdots, x^{(0)}(n))$. After processing, the sequence $X^{(0)} = (X_1^{(0)}, X_2^{(0)}, \cdots X_m^{(0)})^T$ can be reconstructed, where $X_j^{(0)} = (X_j^{(0)}(1), X_j^{(0)}(2), \cdots X_j^{(0)}(n))^T, j = 1, 2 \cdots m$ and m represents the number of cycles. For quarterly data, $m = 4$; for monthly data, $m = 12$.

2.2.2. Fractional order accumulation

Assume that $X^{(0)} = (x^{(0)}(1), x^{(0)}(2), \cdots, x^{(0)}(n))$ is a raw sequence. Then, its r-order fractional accumulation sequence (r-FOA) is $X^{(r)} = (x^{(r)}(1), x^{(r)}(2), \ldots, x^{(r)}(n)), r \in R^+$, where

$$X^{(r)} = A^r X^{(0)} \tag{8}$$

$$A^r = \begin{pmatrix} \begin{bmatrix} r \\ 0 \end{bmatrix} & 0 & 0 & \cdots & 0 \\ \begin{bmatrix} r \\ 1 \end{bmatrix} & \begin{bmatrix} r \\ 0 \end{bmatrix} & 0 & \cdots & 0 \\ \begin{bmatrix} r \\ 2 \end{bmatrix} & \begin{bmatrix} r \\ 1 \end{bmatrix} & \begin{bmatrix} r \\ 0 \end{bmatrix} & \cdots & 0 \\ \vdots & \vdots & \vdots & \ddots & \vdots \\ \begin{bmatrix} r \\ n-1 \end{bmatrix} & \begin{bmatrix} r \\ n-2 \end{bmatrix} & \begin{bmatrix} r \\ n-3 \end{bmatrix} & \cdots & \begin{bmatrix} r \\ 0 \end{bmatrix} \end{pmatrix} \tag{9}$$

Here, $\begin{bmatrix} r \\ i \end{bmatrix} = \frac{r(r+1)\cdots(r+i-1)}{i} = \begin{pmatrix} r+i-1 \\ i \end{pmatrix} = \frac{(r+i-1)!}{i!(r-1)!}$, and $\begin{bmatrix} 0 \\ i \end{bmatrix} = 0, \begin{bmatrix} 0 \\ 0 \end{bmatrix} = \begin{pmatrix} 0 \\ 0 \end{pmatrix} = 1$.

Assume that the raw sequence is $X^{(0)} = (x^{(0)}(1), x^{(0)}(2), \cdots, x^{(0)}(n))$ and its r-order inverse fractional accumulation sequence (r-IFOA) is $X^{(-r)} = (x^{(-r)}(1), x^{(-r)}(2), \ldots, x^{(-r)}(n)), r \in R^+$, where

$$X^{(-r)} = D^r X^{(0)} \tag{10}$$

$$D^r = \begin{pmatrix} \begin{bmatrix} -r \\ 0 \end{bmatrix} & 0 & 0 & \cdots & 0 \\ \begin{bmatrix} -r \\ 1 \end{bmatrix} & \begin{bmatrix} -r \\ 0 \end{bmatrix} & 0 & \cdots & 0 \\ \begin{bmatrix} -r \\ 2 \end{bmatrix} & \begin{bmatrix} -r \\ 1 \end{bmatrix} & \begin{bmatrix} -r \\ 0 \end{bmatrix} & \cdots & 0 \\ \vdots & \vdots & \vdots & & \vdots \\ \begin{bmatrix} -r \\ n-1 \end{bmatrix} & \begin{bmatrix} -r \\ n-2 \end{bmatrix} & \begin{bmatrix} -r \\ n-3 \end{bmatrix} & \cdots & \begin{bmatrix} -r \\ 0 \end{bmatrix} \end{pmatrix} \tag{11}$$

Here, $\begin{bmatrix} -r \\ i \end{bmatrix} = \frac{-r(-r+1)\cdots(-r+i-1)}{i} = (-1)^i \begin{pmatrix} r-i+1 \\ i \end{pmatrix} = (-1)^i \frac{i(r-i+1)!}{i!(r+1)!}$, and $\begin{bmatrix} -r \\ 0 \end{bmatrix} = 0, \begin{bmatrix} 0 \\ 0 \end{bmatrix} = \begin{pmatrix} 0 \\ 0 \end{pmatrix} = 1, i > r$.

Matrix A^r and matrix D^r satisfy $A^r D^r = I_n$.

2.2.3. Construction of FSGM (1,1, α)

After data restart processing, the sequence $X^{(0)} = (x^{(0)}(1), x^{(0)}(2), \cdots, x^{(0)}(n))$ is rearranged as $X^{(0)} = (X_1^{(0)}, X_2^{(0)}, \cdots X_m^{(0)})^T$, $X_j^{(0)} = (x_j^{(0)}(1), x_j^{(0)}(2), \cdots x_j^{(0)}(n))^T, j = 1, 2 \cdots m$, where m represents the number of cycles. If the data are quarterly, then $m = 4$; if the data are

monthly, then $m = 12$. j represents the year. The fractional order accumulation sequence can be represented as $X^{(\alpha)} = (X_1^{(\alpha)}, X_2^{(\alpha)}, \cdots X_m^{(\alpha)})^T$, where $X_j^{(\alpha)} = (X_j^{(\alpha)}(1), X_j^{(\alpha)}(2), \cdots X_j^{(\alpha)}(n))^T, j = 1, 2 \cdots m$. The relationship between $X_j^{(0)}$ and $X_j^{(\alpha)}$ can be expressed as $X_j^{(\alpha)} = A^{\alpha} X_j^{(0)}$.

The whitening equation expression in FSGM (1,1, α) is

$$\frac{dx_m^{(\alpha)}(t)}{dt} + ax_m^{(\alpha)}(t) = b_m \tag{12}$$

Next, we can obtain the following time response functions:

$$x_m^{(\alpha)}(k) = \left(x_m^{(0)}(1) - \frac{b_m}{a}\right) e^{a(1-k)} + \frac{b_m}{a} \tag{13}$$

Now, the following reduction equation can be established:

$$x_m^{(\alpha)}(k) - x_m^{(\alpha)}(k-1) + az_m^{(\alpha)}(k) = b_m, k = 2, 3 \cdots n \tag{14}$$

The background value is $z_m^{(\alpha)}(k) = \lambda_m x_m^{(\alpha)}(k) + (1 - \lambda_m) x_m^{(\alpha)}(k+1)$. In the reduction equation, there are a total of $m+1$ parameters, which are $a, b_1, b_2, \cdots, b_m$. By using the least squares method, we can obtain the following parameters:

$$(a, b_1, b_2, \cdots, b_m)^T = \left(B^T B\right)^{-1} B^T Y \tag{15}$$

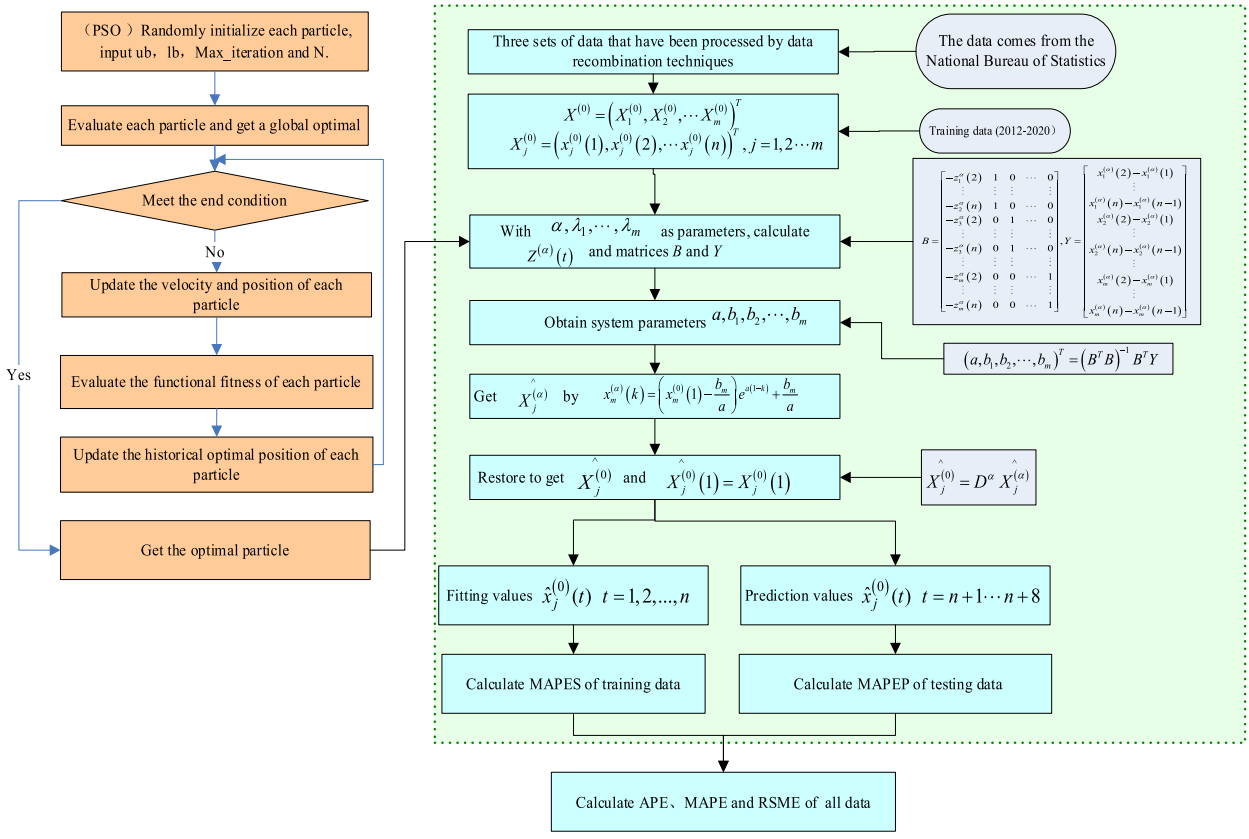

Fig. 2. The modeling process of FSGM (1,1, α).

$$B=\begin{bmatrix} & & & & \\ -z_1^{\alpha}(2) & 1 & 0 & \cdots & 0 \\ \vdots & \vdots & \vdots & & \vdots \\ -z_1^{\alpha}(n) & 1 & 0 & \cdots & 0 \\ -z_2^{\alpha}(2) & 0 & 1 & \cdots & 0 \\ \vdots & \vdots & \vdots & & \vdots \\ -z_2^{\alpha}(n) & 0 & 1 & \cdots & 0 \\ \vdots & \vdots & \vdots & & \vdots \\ -z_m^{\alpha}(2) & 0 & 0 & \cdots & 1 \\ \vdots & \vdots & \vdots & & \vdots \\ -z_m^{\alpha}(n) & 0 & 0 & \cdots & 1 \\ & & & & \end{bmatrix}, Y=\begin{bmatrix} \\ x_1^{(\alpha)}(2)-x_1^{(\alpha)}(1) \\ \vdots \\ x_1^{(\alpha)}(n)-x_1^{(\alpha)}(n-1) \\ x_2^{(\alpha)}(2)-x_2^{(\alpha)}(1) \\ \vdots \\ x_2^{(\alpha)}(n)-x_2^{(\alpha)}(n-1) \\ \vdots \\ x_m^{(\alpha)}(2)-x_m^{(\alpha)}(1) \\ \vdots \\ x_m^{(\alpha)}(n)-x_m^{(\alpha)}(n-1) \end{bmatrix} \mathrm{c} \tag{16}$$

Therefore, the time response function $\widehat{X_j^{(\alpha)}}$ is calculated to obtain $\widehat{X_j^{(0)}} = D^{\alpha}\widehat{X_j^{(\alpha)}}$.

2.2.4. Optimization of the fractional order and background values

In the above process, the fractional order α and background value coefficient $\lambda_1, \lambda_2, \cdots, \lambda_m$ can directly affect the values of parameters $a, b_1, b_2, \cdots, b_m$, thereby affecting the forecasting accuracy. Thus, choosing a reliable fractional order is crucial for improving modeling accuracy. In this paper, PSO is used to determine the optimal parameters via the following steps.

Every optimization problem's solution corresponds to a separate PSO algorithm, that is, a particle. Specifically, the first particle's position is represented by $i, (i = 1,2,\cdots,m)$, $X_i = \{x_i^1, x_i^2, \cdots, x_i^d\}, (d = 1,2,\cdots,D)$, and the velocity is represented by $V_i = \{v_i^1, v_i^2, \cdots, v_i^d\}$. By combining their own experiences *pbest* and those of others *gbest*, the position and velocity of particles are dynamically modified. After several adjustments, the best position of a particle is ultimately given by $P_i = \{p_i^1, p_i^2, \cdots, p_i^d\}$, and the swarm's best position is represented by $G_i = \{g_i^1, g_i^2, \cdots, g_i^d\}$. Furthermore, the equations used to update the position and velocity of each particle are shown in formulas (17) and (18).

$$x_i^d = uv_i^d + c_1 r_1\left(p_i^d - x_i^d\right) + c_2 r_2\left(g_i^d - x_i^d\right) \tag{17}$$

$$v_i^d = x_i^d + v_i^d \tag{18}$$

where m is the number of particles, D is the dimensionality of the search space, u is the inertia factor, and the learning factors c_1 and c_2 denote the weights of the random acceleration terms. r_1 and r_2 are random numbers generated in the range of [0, 1].

2.3. Modeling process

The modeling process of FSGM (1,1, α) is shown in Fig. 2.

2.4. Error evaluation

For numerical simulation results, accuracy verification should generally be performed [37–42]. Therefore, we evaluate the forecasting performance of FSGM(1,1, α) using the absolute percentage error (APE), mean absolute percentage error in the simulation stage (MAPES), average absolute percentage error in the prediction stage (MAPEP), mean absolute percentage error (MAPE) and root mean square error (RMSE). Table 1 presents the corresponding formulas. The evaluation standards for MAPE are shown in Table 2.

Table 1
Error metrics.

Error type	Formula
APE	$APE = \frac{\left\|\widehat{x}^{(0)}(k) - x^{(0)}(k)\right\|}{x^{(0)}(k)} \times 100\%$
MAPES	$MAPES = \frac{1}{n}\sum_{k=1}^{n} APE(k) = \frac{1}{n}\sum_{k=1}^{n} \frac{\left\|\widehat{x}^{(0)}(k) - x^{(0)}(k)\right\|}{x^{(0)}(k)} \times 100\%$
MAPEP	$MAPEP = \frac{1}{f}\sum_{k=n+1}^{n+f} APE(k) = \frac{1}{n}\sum_{k=n+1}^{n+f} \frac{\left\|\widehat{x}^{(0)}(k) - x^{(0)}(k)\right\|}{x^{(0)}(k)} \times 100\%$
MAPE	$MAPE = \frac{1}{n+f}\sum_{k=1}^{n+f} APE(k) = \frac{1}{n}\sum_{k=1}^{n+f} \frac{\left\|\widehat{x}^{(0)}(k) - x^{(0)}(k)\right\|}{x^{(0)}(k)} \times 100\%$
RMSE	$RMSE = \sqrt{\frac{1}{n}\sum_{k=1}^{n}(x^{(0)}(k) - \widehat{x^{(0)}(k)})^2} \times 100\%$

Table 2
Evaluation standards for the MAPE.

MAPE (%)	Forecasting performance
<5	Excellent
5–15	Good
15–50	Reasonable
>50	Incorrect

Models with small MAPEs perform better in prediction tasks than those with large MAPEs.

3. Validation of FSGM (1,1, α)

In this section, we select three sets of seasonal time series data to test the model's effectiveness. These data are sourced from the National Bureau of Statistics and include quarterly power generation in Beijing, China, from 2012 to 2022, quarterly power generation in Henan Province, China, from 2012 to 2022, and quarterly petroleum coke production in China from 2012 to 2022. Moreover, we select GM (1,1), SGM (1,1) [19], DGGM (1,1) [44], DGSM (1,1) [2], and DGSTM (1,1) [20] as competitive models to verify the effectiveness of FSGM (1,1, α).

3.1. Case 1: power generation in Beijing

Power generation reflects the energy supply and demand of a country or region and is closely related to production and consumption in various industries. Therefore, analyzing the growth trend of power generation can help us understand the economic growth of a certain region. The quarterly power generation in Beijing, China, from 2012 to 2022 is used to obtain future generation predictions. The dataset includes a total of 44 time points. We select the first 36 data points (2012–2020) as the training set and the last 8 data points (2021–2022) as the test set for modeling. Table 3 displays the parameter values for the six comparative models. The background value coefficients and fractional order parameter values of FSGM (1,1, α) are obtained using the PSO algorithm and are $\lambda_1 = 0, \lambda_2 = 0, \lambda_3 = 1, \lambda_4 = 0$ and $\widehat{\alpha} = 0.7328$.

The prediction results of the six models based on the original sequence are shown in Fig. 3. The changes in the six predicted sequences generally increase, which is in accordance with the increasing trend of the original sequence. In the traditional GM (1,1), the curve of the entire prediction sequence displays an approximately straight upward trend, reflecting only the approximate trend of the sequence. The poor fitting and prediction results do not reflect the seasonal characteristics of the initial electricity generation, which is why many scholars continue to develop model improvements to adapt to the characteristics of different forecasting data. Notably, in the curves obtained with FSGM (1,1, α), SGM (1,1), DGGM (1,1), DGSM (1,1), and DGSTM (1,1), the electricity generation in each year and quarter displays similar volatility, reflecting why we introduce seasonal characteristics into the grey model. From the trend in the figures, compared with the other models, FSGM (1,1, α) is most suitable for obtaining predictions based on the original sequence. Notably, there are significant gaps between the predicted series and the actual series in the fourth quarter of 2015 and the first quarter of 2016. These gaps are due to the sharp increase in electricity consumption in Beijing at these times based on weather patterns and other natural factors. Moreover, at the single-point scale, the predictions of FSGM (1,1, α) display the smallest difference from the real sequence, so compared with other models, FSGM (1,1, α) is is most suitable for predicting the power generation in Beijing.

Table 4 shows the maximum APE values in the simulation and prediction stages, indicating that FSGM(1,1) achieves good predictive performance. In the simulation phase, the maximum APE value of FSGM (1,1, α) is 20.07 %, with a relatively low simulation error and an absolute advantage. For the prediction stage, the maximum APE value of FSGM (1,1, α) is 10.69 %, which is slightly larger than the value of 9.43 % obtained with DGSTM (1,1), and the proposed model displays certain advantages compared to other models. In addition, GM (1,1) without seasonal features produces large prediction errors for seasonal data, and the error of SGM (1,1) when applying seasonal factors to process data is relatively low.

Moreover, box plots of the APE values are shown in Fig. 4. We can see that FSGM (1,1, α) achieves good predictive performance for the original sequence compared to the other models. Specifically, the variation range of the APE values of FSGM (1,1, α) is [0, 20 %],

Table 3
Parameter estimates for case 1.

Model	Parameter value
FSGM(1,1, α)	$\alpha = 0.7328, \lambda_1 = 0, \lambda_2 = 0, \lambda_3 = 1, \lambda_4 = 0$ $\widehat{a} = 0.0276, \widehat{b}_1 = 76.3046, \widehat{b}_2 = 48.5634, \widehat{b}_3 = 67.6595, \widehat{b}_4 = 74.4036$
GM(1,1)	$\widehat{a} = -0.0115, \widehat{b} = 78.4766$
SGM(1,1)	$\widehat{a} = -0.0124, \widehat{b} = 78.2813$
DGGM(1,1)	$\widehat{a}_1 = -0.0338, \widehat{a}_2 = -0.0385, \widehat{a}_3 = -0.0348, \widehat{a}_4 = -0.0346$ $\widehat{b}_1 = 102.6101, \widehat{b}_2 = 63.2446, \widehat{b}_3 = 88.0607, \widehat{b}_4 = 99.3082$
DGSM(1,1)	$\widehat{a} = 1.0106, \widehat{b}_1 = 99.5455, \widehat{b}_2 = 53.2102, \widehat{b}_3 = 78.8220, \widehat{b}_4 = 92.5385$
DGSTM(1,1)	$\widehat{a} = 0.9051, \widehat{b} = 10.5323$ $\widehat{c}_1 = 81.3362, \widehat{c}_2 = 38.5194, \widehat{c}_3 = 60.9410, \widehat{c}_4 = 74.2518$

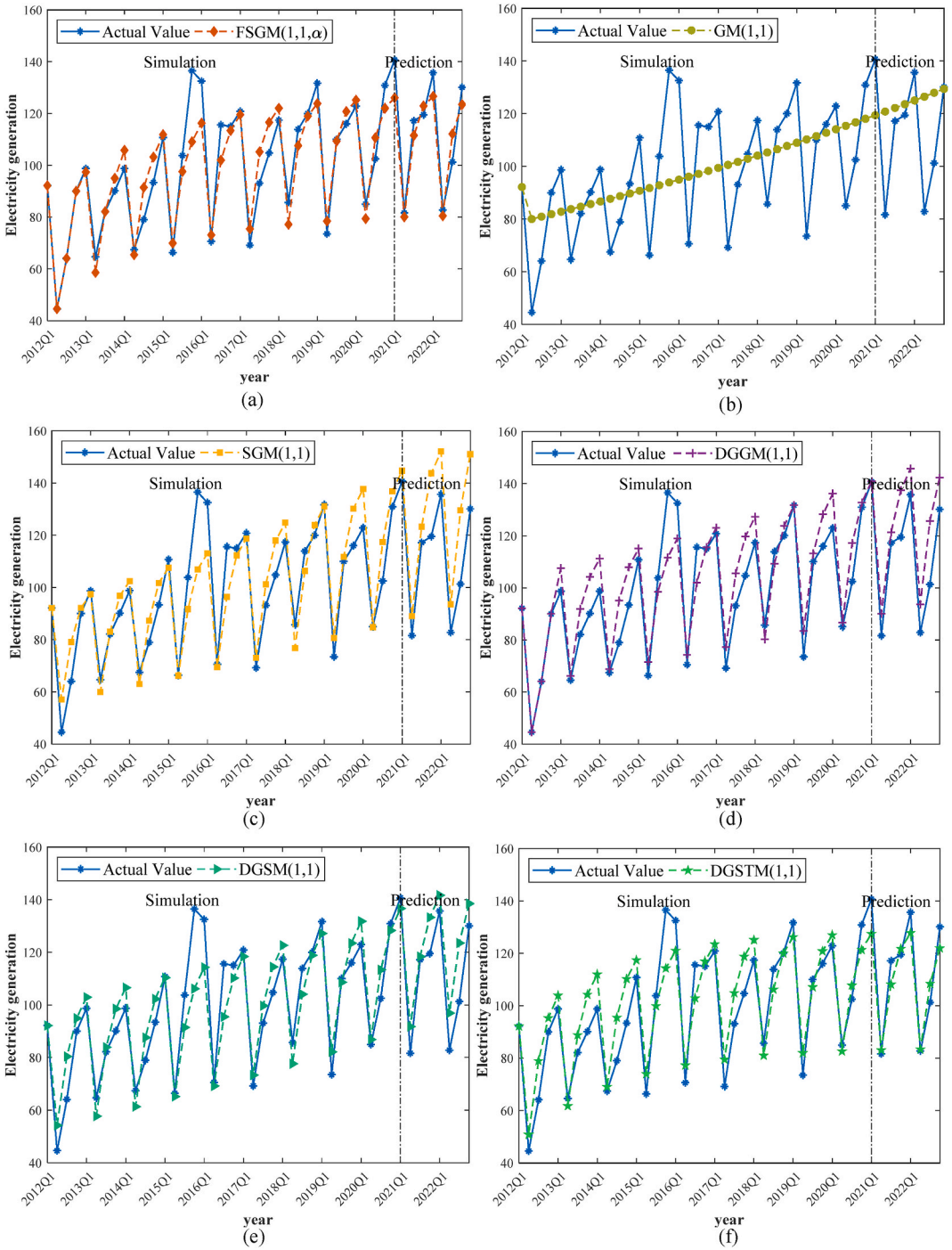

Fig. 3. Simulation and prediction curves for case 1. (a) FSGM (1,1, α); (b) GM(1,1); (c) SGM (1,1); (d) DGGM (1,1), (e) DGSM (1,1); (f) DGSTM (1,1).

Table 4
Maximum APE values for case 1.

%		FSGM(1,1, α)	GM(1,1)	SGM(1,1)	DGGM(1,1)	DGSM(1,1)	DGSTM(1,1)
APE_Max	Simulation	20.07	79.43	28.04	20.46	25.44	23.25
	Prediction	10.69	52.74	27.91	24.02	21.94	9.43

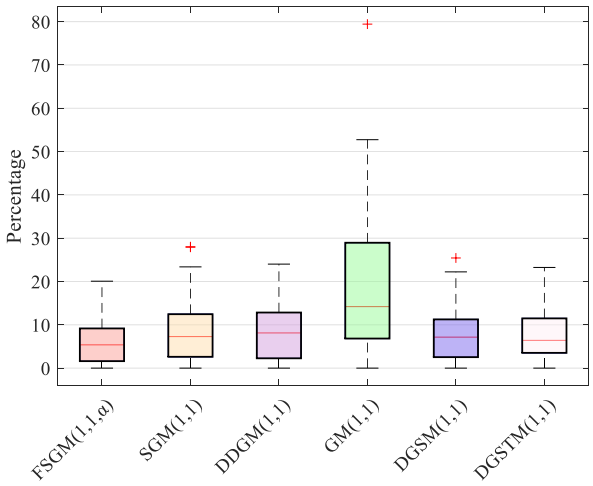

Fig. 4. Box plots of the APE values for case 1.

and the data are relatively concentrated in [0, 10 %], with a lower fluctuation amplitude than those of the other five models. In addition, SGM (1,1), GM (1,1), and DGSM (1,1) all produce some abnormal data, enhancing the prediction of volatile APE values in these three models. Table 5 lists the specific RMSE, MAPE, MAPES, and MAPEP values. Compared with the other models, FSGM (1,1, α) yields the smallest RMSE, MAPE, and MAPES values. Additionally, the MAPEP value is 4.98 %, which is slightly higher than the value of 4.45 % obtained for DGSTM (1,1). Furthermore, GM (1,1) displays poor predictive ability for seasonal data, indicating that it is not suitable for predicting data with periodic fluctuations.

3.2. Case 2: power generation in Henan Province

In this section, we use the quarterly power generation in Henan Province, China, from 2012 to 2022 for corresponding prediction research. This dataset includes a total of 44 data points. We select the first 36 data points (2012–2020) as the training set and the last 8 data points (2021–2022) as the test set for modeling. The parameter values of the six compared models are presented in Table 6. PSO is applied to obtain the background value coefficients and fractional order parameter values of FSGM (1,1, α), which are $\lambda_1 = 0.6244$, $\lambda_2 = 0.7840, \lambda_3 = 1, \lambda_4 = 0.5265$ and $\widehat{\alpha} = 1.1420$.

The predicted sequences of the six models are shown in Fig. 5. The trends of the six predicted sequences increase, which is in accordance with the increasing trend of the original sequence. However, the increase is small, indicating that electricity consumption in Henan Province has been relatively stable over the past 10 years. For the results of the traditional GM (1,1), the curve of the entire prediction sequence approximates a straight line, reflecting the approximate trend; moreover, the fitting and prediction effects are poor and cannot reflect the seasonal characteristics of initial electricity generation. Notably, in the curves predicted by the FSGM (1,1), SGM (1,1), DGGM (1,1), DGSM (1,1), and DGSTM (1,1) models, electricity generation in each year and quarter displays similar volatility, highlighting the value of adding seasonal features to grey models. From the trends in the graphs, FSGM (1,1, α) fits the original sequence better than the other competing models. There is a significant gap between the predicted and actual series of electricity consumption in the third quarter since 2017. The possible reason is that with economic development, people's living conditions have gradually improved. The hot weather in the third quarter led to a sharp increase in electricity consumption in Henan Province, as residents reduced their electricity consumption. At the same time, at the single-point scale, the predictions of FSGM (1,1, α) display the smallest difference from the real sequence; therefore, compared with other models, FSGM (1,1, α) is the most suitable for predicting the power generation in Henan Province.

Table 7 shows the maximum APE values in the simulation and prediction stages, indicating that FSGM(1,1, α) achieves good predictive performance. In the simulation phase, the maximum APE value of FSGM (1,1, α) is 14.08 %, and the advantage over other models is not significant. However, in the prediction phase, the maximum APE value of FSGM (1,1, α) is 13.93 %, and the absolute

Table 5
Errors metrics for case 1.

Model	RMSE	MAPE(%)	MAPES(%)	MAPEP(%)
FSGM(1,1, α)	8.10	5.78	5.81	4.98
GM(1,1)	20.71	19.12	18.97	20.45
SGM(1,1)	11.61	8.85	7.86	14.81
DGGM(1,1)	10.34	8.04	7.53	11.81
DGSM(1,1)	10.04	8.19	7.85	10.70
DGSTM(1,1)	9.00	7.80	8.40	4.45

Table 6
Parameter estimates for case 2.

Model	Parameter value
FSGM(1,1, α)	$\alpha = 1.1420, \lambda_1 = 0.6244, \lambda_2 = 0.7840, \lambda_3 = 1, \lambda_4 = 0.5265$ $\widehat{a} = -0.0337, \widehat{b}_1 = 752.1014, \widehat{b}_2 = 718.8536, \widehat{b}_3 = 818.9975, \widehat{b}_4 = 752.9340$
GM(1,1)	$\widehat{a} = -0.0013, \widehat{b} = 666.5734$
SGM(1,1)	$\widehat{a} = -0.0013, \widehat{b} = 666.8008$
DGGM(1,1)	$\widehat{a}_1 = 0.0068, \widehat{a}_2 = -0.0021, \widehat{a}_3 = -0.0130, \widehat{a}_4 = -0.0040$ $\widehat{b}_1 = 692.1499, \widehat{b}_2 = 643.8922, \widehat{b}_3 = 710.2366, \widehat{b}_4 = 684.2010$
DGSM(1,1)	$\widehat{a} = 1.0012, \widehat{b}_1 = 659.3278, \widehat{b}_2 = 634.1488, \widehat{b}_3 = 723.0858, \widehat{b}_4 = 655.0158$
DGSTM(1,1)	$\widehat{a} = 0.9240, \widehat{b} = 52.5465$ $\widehat{c}_1 = 655.4645, \widehat{c}_2 = 630.2572, \widehat{c}_3 = 716.6744, \widehat{c}_4 = 653.0115$

advantage of this model over the other models is evident. Overall, FSGM(1,1, α) outperforms the other competitive models. The prediction results also reveal that GM (1,1) yields a large prediction error for seasonal data, and in comparison, SGM (1,1) yields a relatively significant reduction in error.

Moreover, box plots of the APE values are shown in Fig. 6. Specifically, the range of APE values for FSGM (1,1, α) is [0, 12 %], and the data are relatively concentrated in the range of [0, 3 %]. The fluctuation in amplitude for these results is lower than that for the results of the other five models, indicating that FSGM (1,1, α) provides more reliable predictive ability than the other models. Table 8 shows the specific values of the RMSE, MAPE, MAPES, and MAPEP for the six models. The four indicators for FSGM (1,1, α) are all lower than those of the other models, indicating that FSGM (1,1, α) achieves better predictive performance based on the original sequence. Similarly, GM (1,1) displays poor predictive ability for seasonal data, indicating that it is not suitable for predicting data with periodic fluctuations.

3.3. Case 3: petroleum coke production in China

As an important fossil energy and chemical raw material, petroleum coke has a profound impact on various industries. Therefore, we use the quarterly production of Chinese petroleum coke from 2012 to 2022 for corresponding prediction research. This dataset includes a total of 44 data points. We select the first 36 data points (2012–2020) as the training set and the last 8 data points (2021–2022) as the test set for modeling. The parameter values are presented in Table 9. PSO is applied to obtain the background value coefficients and fractional order parameter values of FSGM (1,1, α), which are $\lambda_1 = 0.4625, \lambda_2 = 1, \lambda_3 = 0.3871, \lambda_4 = 0$ and $\widehat{\alpha} = 0.9815$.

The predicted sequences of the six models are shown in Fig. 7. The changes in the six predicted sequences increase, consistent with the increasing trend of the original sequence. In the traditional GM (1,1), the curve of the entire prediction sequence approximates a straight line, reflecting the original trend only approximately, and the fitting and prediction effects are poor; therefore, the seasonal characteristics of the initial coke production are poorly modeled. Notably, in the curves predicted by the FSGM (1,1), SGM (1,1), DGGM (1,1), DGSM (1,1), and DGSTM (1,1) models, coke production in each year and quarter displays similar volatility, highlighting the value in adding seasonal features to the models. The trend in the graph shows that FSGM (1,1, α) yields a significantly better fit for the raw data than the other competing models. The difference between the actual sequences and that predicted by the FSGM (1,1, α) model is significantly smaller than that of the other models; therefore, compared with the other models, FSGM (1,1, α) is the most suitable for predicting the petroleum coke production in China.

Moreover, box plots of the APE values are shown in Fig. 8. Specifically, the range of APE values for FSGM (1,1, α) is [0, 7 %], and the data are relatively concentrated in the range of [0, 2 %]. The fluctuation in amplitude for these results is lower than that for the results of the other five models, indicating that FSGM (1,1, α) provides more reliable predictive ability than the other models. Table 10 shows the maximum APE values in the simulation and prediction stages, indicating that FSGM (1,1, α) achieves good predictive performance. In the simulation and prediction stages, the maximum APE values of FSGM(1,1, α) are 11.46 % and 3.13 %, respectively, the smallest values observed, indicating that FSGM(1,1, α) has an absolute advantage over other competitive models. The prediction results also reveal that GM (1,1) yields a large prediction error for seasonal data, and in comparison, SGM (1,1) produces a relatively significant reduction in error. Table 11 shows the specific values of the RMSE, MAPE, MAPES, and MAPEP for the six models. These four for FSGM (1,1, α) are lower than those for the other models, indicating that FSGM (1,1, α) achieves better predictive performance for the raw sequence. Similarly, GM (1,1) exhibits poor predictive ability for seasonal data, indicating that it is not suitable for predicting data with periodic fluctuations.

4. Prediction results

Based on analyses of the above three cases, it is found that FSGM (1,1, α) can effectively capture the seasonal characteristics of the original sequences and yields the best simulation and prediction performance. Therefore, based on the results above, FSGM (1,1, α) is applied to predict quarterly electricity generation in Beijing and Henan Provinces and petroleum coke production in China from 2023 to 2027. The prediction results are shown in Table 12 and Fig. 9. From 2023 to 2027, electricity generation in Beijing and Henan Provinces and petroleum coke production in China display obvious cyclical seasonal fluctuations. Notably, power generation in Beijing

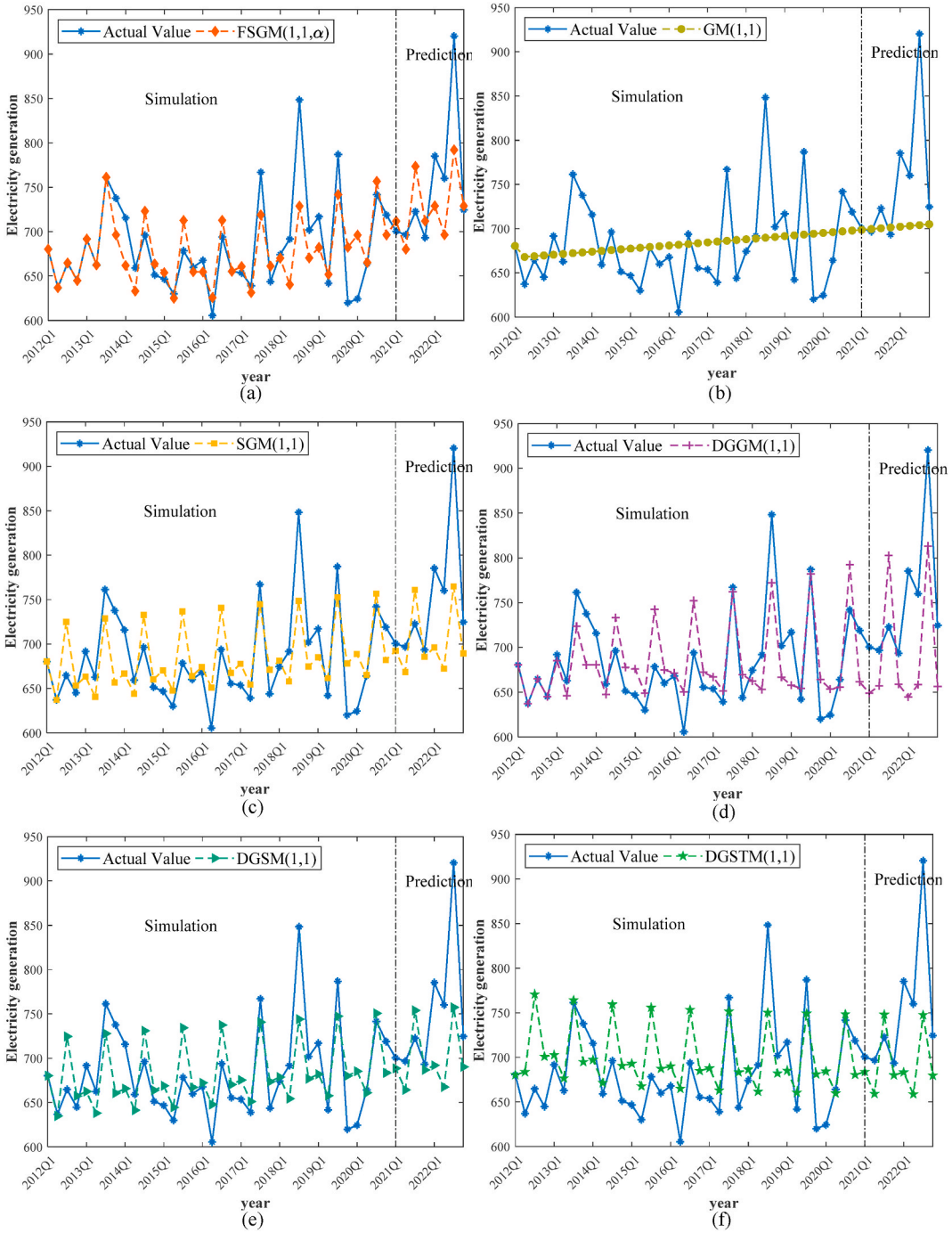

Fig. 5. Simulation and prediction curves for case 2. (a) FSGM (1,1, α); (b) GM(1,1); (c) SGM (1,1); (d) DGGM (1,1), (e) DGSM (1,1); (f) DGSTM (1,1).

Table 7
Maximum APE values for case 2.

		FSGM(1,1, α)	GM(1,1)	SGM(1,1)	DGGM(1,1)	DGSM(1,1)	DGSTM(1,1)
APE_Max	Simulation	14.08	18.70	11.75	9.46	12.28	15.93
	Prediction	13.93	23.51	16.89	17.94	17.71	18.78

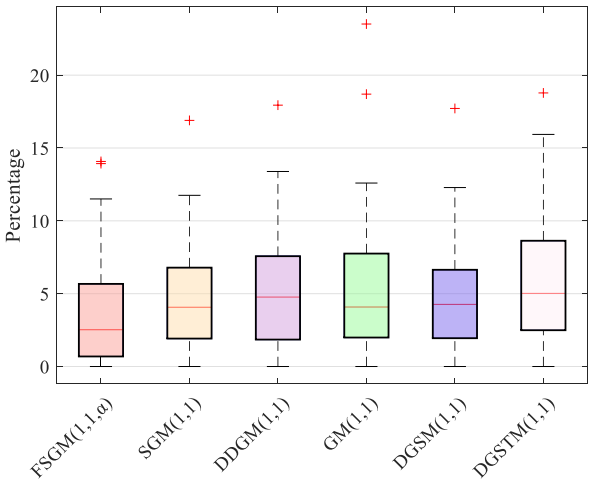

Fig. 6. Box plots of the APE values for case 2.

Table 8
Error metrics for Case 2.

Model	RMSE	MAPE(%)	MAPES(%)	MAPEP(%)
FSGM(1,1, α)	39.63	3.62	3.21	6.02
GM(1,1)	58.13	5.61	5.49	7.00
SGM(1,1)	46.32	4.80	4.30	7.87
DGGM(1,1)	47.67	5.01	3.86	10.59
DGSM(1,1)	47.26	4.85	4.32	8.06
DGSTM(1,1)	53.26	5.84	5.35	8.87

Table 9
Parameter estimates for case 3.

Model	Parameter value
FSGM(1,1, α)	$\alpha = 0.9815, \lambda_1 = 0.4625, \lambda_2 = 1, \lambda_3 = 0.3871, \lambda_4 = 0$ $\widehat{a} = -0.0250, \widehat{b}_1 = 5.4876 \times 10^6, \widehat{b}_2 = 5.4714 \times 10^6, \widehat{b}_3 = 5.5460 \times 10^6, \widehat{b}_4 = 5.8789 \times 10^6$
GM(1,1)	$\widehat{a} = -0.0091, \widehat{b} = 5.3958 \times 10^6$
SGM(1,1)	$\widehat{a} = -0.0091, \widehat{b} = 5.4005 \times 10^6$
DGGM(1,1)	$\widehat{a}_1 = -0.0254, \widehat{a}_2 = -0.0329, \widehat{a}_3 = -0.0279, \widehat{a}_4 = -0.0292$ $\widehat{b}_1 = 5.8408 \times 10^6, \widehat{b}_2 = 5.7365 \times 10^6, \widehat{b}_3 = 5.8452 \times 10^6, \widehat{b}_4 = 6.0804 \times 10^6$
DGSM(1,1)	$\widehat{a} = 1.0091, \widehat{b}_1 = 5.4518 \times 10^6, \widehat{b}_2 = 5.4030 \times 10^6, \widehat{b}_3 = 5.3008 \times 10^6, \widehat{b}_4 = 5.5604 \times 10^6$
DGSTM(1,1)	$\widehat{a} = 0.9392, \widehat{b} = 4.4986 \times 10^5$ $\widehat{c}_1 = 4.8465 \times 10^6, \widehat{c}_2 = 4.8517 \times 10^6, \widehat{c}_3 = 4.7419 \times 10^6, \widehat{c}_4 = 4.9908 \times 10^6$

fluctuates between 8 and 12.7 billion kilowatt hours, maintaining a relatively stable level and without significant growth. Power generation in Henan Province exhibits a continuous growth trend, increasing from 74.648 billion kilowatt hours in the fourth quarter of 2023 to 83.241 billion kilowatt hours in the fourth quarter of 2027, an increase of 11.50 %. Petroleum coke production in China also exhibits a continuous growth trend, increasing from 8.2 million tons in the fourth quarter of 2023 to 9.1 million tons in the fourth quarter of 2027, an increase of 10.93 %.

5. Conclusion

In response to the shortcomings of the existing grey season models and to accurately predict sequence data with seasonal characteristics, we combine data restart technology and fractional order accumulation and propose a new grey season model: FSGM (1,1, α). On this basis, the PSO algorithm is used to solve for the fractional order and background value coefficients of FSGM (1,1, α), and the effectiveness of FSGM (1,1, α) is verified through three cases. Finally, we use FSGM (1,1) to predict quarterly electricity generation in Beijing and Henan Provinces and petroleum coke production in China from 2023 to 2027. The research results indicate that the modeling method and solution process of FSGM (1,1, α) are reasonable and effective and can effectively capture the dynamic trends of seasonal data. Second, compared with the traditional GM (1,1), SGM (1,1), DGGM (1,1), DGSM (1,1), and DGSTM (1,1) models with seasonal characteristics, FSGM (1,1, α) can better fit the original data, achieves higher prediction accuracy, and performs better. Third,

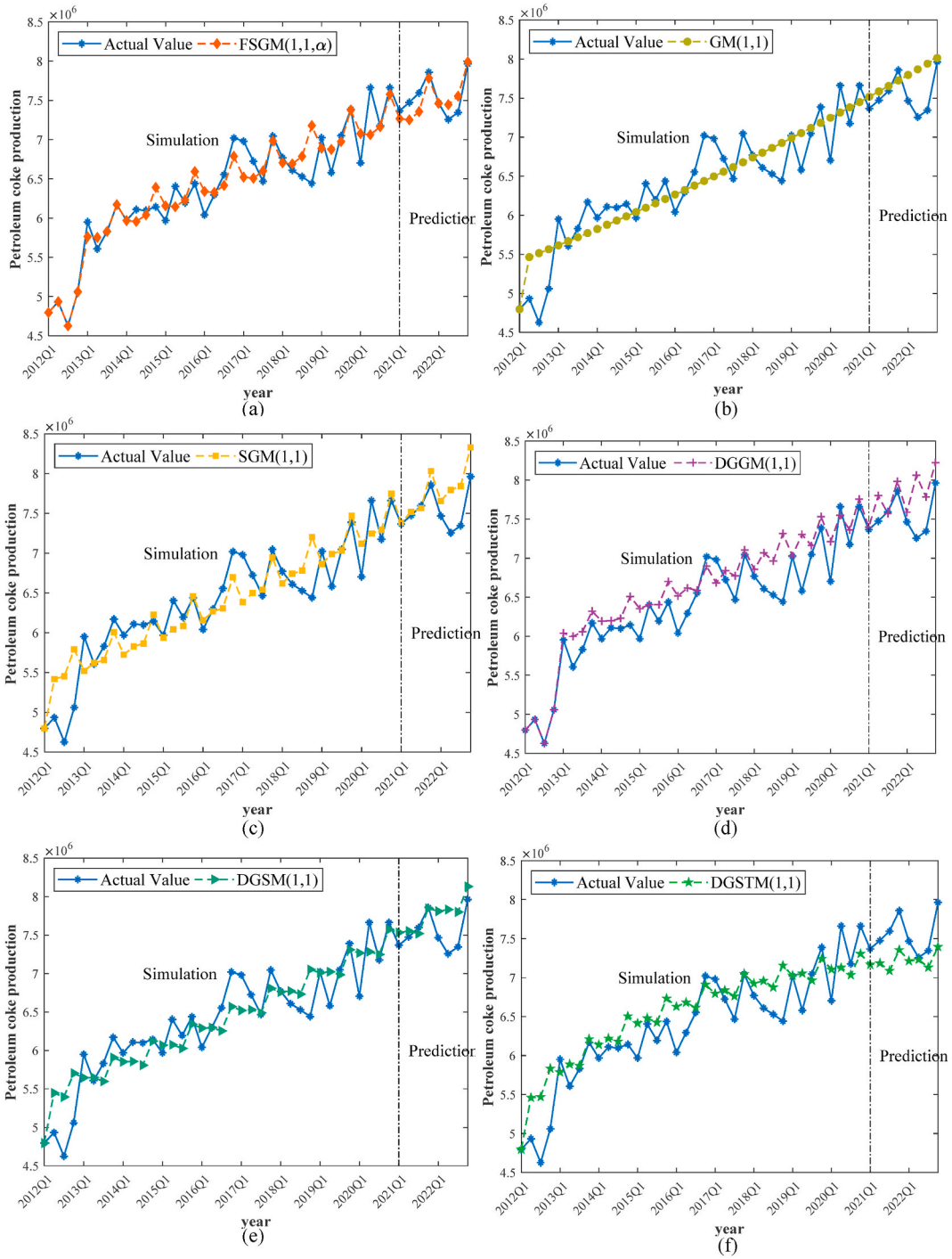

Fig. 7. Simulation and prediction curves for case 3. (a) FSGM (1,1, α); (b) GM(1,1); (c) SGM (1,1); (d) DGGM (1,1), (e) DGSM (1,1); (f) DGSTM (1,1).

from 2023 to 2027, electricity generation in Beijing and Henan Provinces and petroleum coke production in China all exhibit significant cyclical seasonal fluctuations. The trend of power generation in Beijing is relatively stable, while the trends of power generation in Henan Province and petroleum coke production in China exhibit certain steady upward growth. It is expected that power generation in Henan Province and petroleum coke production in China in the fourth quarter of 2027 will increase by 11.50 % and 10.93 %, respectively, compared to the levels in the fourth quarter of 2023.

When solving the model, we divide the data into four groups according to seasonal factors and solve the time response function for

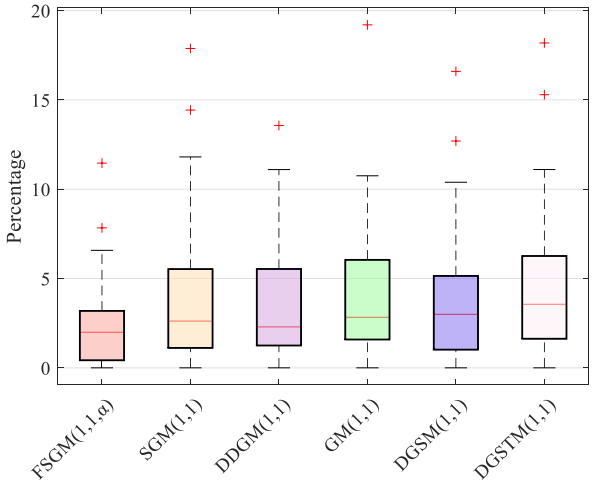

Fig. 8. Box plots of the APE values for case 3.

Table 10
Maximum APE values for case 3.

		FSGM(1,1, α)	GM(1,1)	SGM(1,1)	DGGM(1,1)	DGSM(1,1)	DGSTM(1,1)
APE_Max	Simulation	11.46	19.20	17.88	13.57	16.60	18.19
	Prediction	3.13	8.43	7.41	11.10	7.92	7.14

Table 11
Errors metrics for case 3.

Model	RMSE	MAPE(%)	MAPES(%)	MAPEP(%)
FSGM(1,1, α)	2.215	2.30	2.41	1.85
GM(1,1)	3.300	4.14	4.30	3.65
SGM(1,1)	3.244	3.90	4.07	3.50
DGGM(1,1)	3.144	3.49	3.47	4.04
DGSM(1,1)	3.129	3.85	4.00	3.28
DGSTM(1,1)	3.554	4.48	4.54	4.40

Table 12
Projections from 2023 to 2027.

Time	Power generation in Beijing (100 million kWh)	Power generation in Henan (100 million kWh)	Petroleum coke production in China (10^6 t)
2023Q1	126.93	747.58	7.66
2023Q2	80.72	714.21	7.64
2023Q3	112.46	812.22	7.75
2023Q4	123.77	746.48	8.20
2024Q1	127.00	767.37	7.86
2024Q2	80.80	733.10	7.85
2024Q3	112.58	833.64	7.96
2024Q4	123.83	766.19	8.42
2025Q1	126.87	788.35	8.07
2025Q2	80.76	753.13	8.05
2025Q3	112.51	856.37	8.17
2025Q4	123.71	787.11	8.64
2026Q1	126.57	810.49	8.28
2026Q2	80.60	774.27	8.26
2026Q3	112.29	880.36	8.38
2026Q4	123.42	809.19	8.87
2027Q1	126.13	833.76	8.49
2027Q2	80.35	796.50	8.48
2027Q3	111.93	905.59	8.60
2027Q4	122.99	832.41	9.10

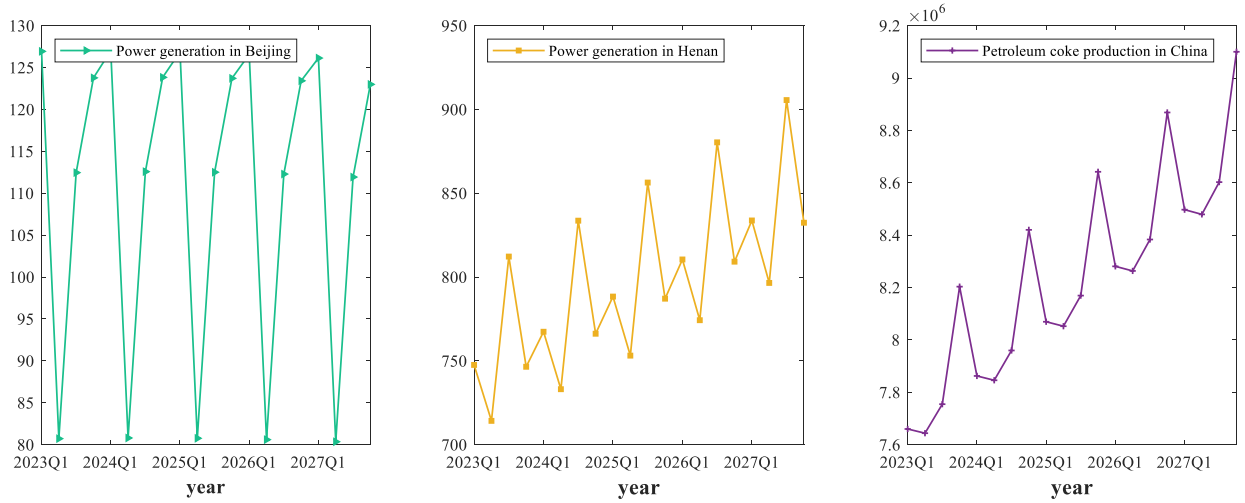

Fig. 9. Predicted curves from 2023 to 2027.

each group separately. Then, we establish the recovery equations used to solve for the five parameters. Although this approach improves the prediction accuracy of the grey model, we may have overlooked the impact between quarters to some extent. For example, if the first-quarter growth does not reach the expected rate, the local government may take corresponding measures to adjust the production plan for the second quarter, which will affect the future development trend. This is a direction for the future improvement of the model.

Nomenclature

r- FOA	r-order fractional accumulation
r-IFOA	r-order inverse accumulative generation operator
GM(1,1)	grey model
SGM (1,1)	seasonal grey model
DGGM (1,1)	data grouping grey model
DGSM	discrete grey seasonal model
DGSTM (1,1)	data grouping seasonal time model
FSGM (1,1, α)	α-order fractional seasonal grey model
PSO	particle swarm optimization
APE	absolute percentage error
MAPE	mean absolute percentage error
RMSE	root mean square error

Funding

This work was supported by the National Social Science Fund of China (No. 23XTJ001), the Shaanxi Soft Science Foundation (2024 ZC-YBXM-102), and the Shaanxi Soft Science Foundation (2024 ZC-YBXM-075).

Additional information

No additional information is available for this paper.

Data availability

Data will be made available on request.

CRediT authorship contribution statement

Huiping Wang: Writing – review & editing, Validation, Supervision, Conceptualization. **Yiyang Li:** Writing – original draft, Software, Methodology, Formal analysis.

Declaration of competing interest

The authors declare that they have no known competing financial interests or personal relationships that could have appeared to influence the work reported in this paper.

References

[1] H. Wang, Z. Zhang, A spatial lagged multivariate discrete grey model for forecasting an economy-energy-environment system, J. Clean. Prod. 404 (2023) 136922.
[2] W. Zhou, S. Ding, A novel discrete grey seasonal model and its applications. Commun. Nonlinear Sci. Numer. Simul. 93 (12021), 05493..
[3] B. Zeng, H. Li, L. Yu, Y. Bai, Feature extraction and fractional grey prediction modeling of seasonal fluctuation data, Syst. Eng. Theory Pract. 42 (2) (2022) 471–486.
[4] C. Liu, H. Zhu, Y. Ren, Z. Wang, A novel intelligent forecasting framework for quarterly or monthly energy consumption, IEEE T. Ind. Inform. 20 (4) (2024) 5352–5363.
[5] X. Wang, N. Xie, L. Yang, A flexible grey Fourier model based on integral matching for forecasting seasonal PM2.5 time series. Chaos Soliton, Fract. 162 (2022) 112417.
[6] S. Ding, Z. Tao, R. Li, X. Qin, A novel seasonal adaptive grey model with the data-restacking technique for monthly renewable energy consumption forecasting, Expert Syst. Appl. 208 (2022) 118115.
[7] W. Zhou, H. Li, Z. Zhang, A novel seasonal fractional grey model for predicting electricity demand (A case study of Zhejiang in China, Math. Comput. Simulat. 200 (2022) 128–147.
[8] Z. Wang, L. He, Y. Zhao, Forecasting the seasonal natural gas consumption in the US using a gray model with dummy variables, Appl. Soft Comput. 113 (2021) 108002.
[9] X. Li, X. Guo, L. Liu, Y. Cao, B. Yang, A novel seasonal grey model for forecasting the quarterly natural gas production in China, Energy Rep. 8 (2022) 9142–9157.
[10] P. Du, J. Guo, S. Sun, S. Wang, J. Wu, A novel two-stage seasonal grey model for residential electricity consumption forecasting, Energy 258 (2022) 124664.
[11] G. Sudheer, A. Suseelatha, Short term load forecasting using wavelet transform combined with Holt-Winters and weighted nearest neighbor models, Int. J. Elec. Power Energy Syst. 64 (2015) 340–346.
[12] E. Yukseltan, A. Yucekaya, A. Bilge, Forecasting electricity demand for Turkey (Modeling periodic variations and demand segregation, Appl. Energy 193 (2017) 287–296.
[13] Q. Mao, K. Zhang, W. Yan, C. Cheng, Forecasting the incidence of tuberculosis in China using the seasonal auto-regressive integrated moving average (SARIMA) model, J. Infecti. Public Heal. 11 (5) (2018) 707–712.
[14] S. Xu, H. Chan, T. Zhang, Forecasting the demand of the aviation industry using hybrid time series SARIMA-SVR approach, Transport Res. E-Log. 122 (2019) 169–180.
[15] J. Bedi, D. Toshniwal, Energy load time-series forecast using decomposition and autoencoder integrated memory network, Appl. Soft Comput. 93 (2020) 106390.
[16] Z. Wang, Y. Zhao, L. He, Forecasting the monthly iron ore import of China using a model combining empirical mode decomposition, non-linear autoregressive neural network, and autoregressive integrated moving average, Appl. Soft Comput. 94 (2020) 106475.
[17] X. Zhang, J. Wang, A novel decomposition-ensemble model for forecasting short-term load-time series with multiple seasonal patterns, Appl. Soft Comput. 65 (2018) 478–494.
[18] Y. Nie, J. Sun, J. Ma, Seasonal prediction of summer extreme precipitation frequencies over Southwest China based on machine learning, Atmos. Res. 294 (2023) 106947.
[19] Z. Wang, Q. Li, L. Pei, A seasonal GM(1, 1) model for forecasting the electricity consumption of the primary economic sectors, Energy 154 (2018) 522–534.
[20] W. Zhou, R. Jiang, S. Ding, Y. Cheng, Y. Li, H. Tao, A novel grey prediction model for seasonal time series, Knowledge-Based Syst. 229 (2021) 107363.
[21] H. Chen, L. Pei, Y. Zhao, Forecasting seasonal variations in electricity consumption and electricity usage efficiency of industrial sectors using a grey modeling approach, Energy 222 (2021) 119952.
[22] N. Li, J. Wang, L. Wu, Y. Bentley, Predicting monthly natural gas production in China using a novel grey seasonal model with particle swarm optimization, Energy 215 (2021) 119118.
[23] X. Xiong, X. Hu, T. Tian, H. Guo, H. Liao, A novel optimized initial condition and seasonal division based grey seasonal variation index model for hydropower generation, Appl. Energy 328 (2022) 120180.
[24] Z. Li, X. Hu, H. Guo, X. Xiong, A novel weighted average weakening buffer operator based fractional order accumulation seasonal grouping grey model for predicting the hydropower generation, Energy 277 (2023) 127568.
[25] X. Meng, L. Tu, C. Yan, L. Wu, Forecast of annual water consumption in 31 regions of China considering GDP and population, Sustain Prod. Consump. 27 (2021) 713–736.
[26] Y. Liu, Y. Yang, F. Pan, D. Xue, A conformable fractional unbiased grey model with a flexible structure and it's application in hydroelectricity consumption prediction, J. Clean. Prod. 367 (2022) 133029.
[27] Y. Wang, L. Wang, L. Ye, X. Ma, W. Wu, Z. Yang, X. He, L. Zhang, Y. Zhang, Y. Zhou, Y. Luo, A novel self-adaptive fractional multivariable grey model and its application in forecasting energy production and conversion of China, Eng Appl. Artif. Intel. 115 (2022) 105319.
[28] H. Wu, S. Liu, J. Du, Z. Fang, A novel grey spatial extension relational model and its application to identify the drivers for ambient air quality in Shandong Province, China, Sci. Total Environ. 845 (2022) 157208.
[29] Y. Yang, X. Wang, A novel modified conformable fractional grey time-delay model for power generation prediction, Chaos Soliton. Fract. 158 (2022) 112004.
[30] W. Wu, X. Ma, B. Zeng, H. Zhang, P. Zhang, A novel multivariate grey system model with conformable fractional derivative and its applications, Comput. Ind. Eng. 164 (2022) 107888.
[31] W. Qian, A. Sui, A novel structural adaptive discrete grey prediction model and its application in forecasting renewable energy generation, Expert Syst. Appl. 186 (2021) 115761.
[32] H. Wang, Z. Zhang, Forecasting Chinese provincial carbon emissions using a novel grey prediction model considering spatial correlation, Expert Syst. Appl. 209 (2022) 118261.
[33] J. Ye, Z. Xu, X. Gou, An adaptive Grey-Markov model based on parameters Self-optimization with application to passenger flow volume prediction, Expert Syst. Appl. 202 (2022) 117302.
[34] H. Zhou, Y. Dang, D. Yang, J. Wang, Y. Yang, An improved grey multivariable time-delay prediction model with application to the value of high-tech industry, Expert Syst. Appl. 213 (2023) 119061.
[35] B. Zeng, H. Li, C. Mao, Y. Wu, Modeling, prediction and analysis of new energy vehicle sales in China using a variable-structure grey model, Expert Syst. Appl. 213 (2023) 118879.
[36] X. Ma, Y. Deng, M. Ma, A novel kernel ridge grey system model with generalized Morlet wavelet and its application in forecasting natural gas production and consumption, Energy 287 (2024) 129630.
[37] W.B. Ye, M. Arıcı, Redefined interface error, 2D verification and validation for pure solid-gallium phase change modeling by enthalpy-porosity methodology, Int. Commun. Heat Mass. 147 (2023) 106952.

[38] W.B. Ye, M. Arıcı, False diffusion, asymmetrical interface, and equilibrious state for pure solid-gallium phase change modeling by enthalpy-porosity methodology, Int. Commun. Heat Mass. 144 (2023) 106746.
[39] W.B. Ye, M. Arıcı, 3D validation, 2D feasibility, corrected and developed correlations for pure solid-gallium phase change modeling by enthalpy-porosity methodology, Int. Commun. Heat Mass. 144 (2023) 106780.
[40] W.B. Ye, M. Arıcı, Exploring mushy zone constant in enthalpy-porosity methodology for accurate modeling convection-diffusion solid-liquid phase change of calcium chloride hexahydrate, Int. Commun. Heat Mass. 152 (152) (2024) 107294.
[41] S.V. Trukhanov, A.V. Trukhanov, V.G. Kostishyn, et al., High-frequency absorption properties of gallium weakly doped barium hexaferrites, Philos. Mag. A 99 (2019) 585–605.
[42] M.A. Almessiere, N.A. Algarou, Y. Slimani, et al., Investigation of exchange coupling and microwave properties of hard/soft (SrNi0. 02Zr0. 01Fe11. 96O19)/(CoFe2O4) x nanocomposites, Mater. Today Nano 18 (2022) 100186.
[43] J. Chen, G. Li, D. Wu, S. Shen, Forecasting seasonal tourism demand using a multiseries structural time series method, J. Travel Res. 58 (1) (2019) 92–103.
[44] Z. Wang, Q. Li, L. Pei, Grey forecasting method of quarterly hydropower production in China based on a data grouping approach, Appl. Math. Model. 51 (2017) 302–316.